Astronomy & Astrophysics manuscript no. newhp1final
April 8, 2016
© ESO 2016

arXiv:1604.02095v1 [astro-ph.SR] 7 Apr 2016

High-resolution abundance analysis of red giants in the metal-poor bulge globular cluster HP 1 ⋆

B. Barbuy[1], E. Cantelli[1], A. Vemado[1], H. Ernandes[1], S. Ortolani[2,3], I. Saviane[4], E. Bica[5], D. Minniti[6,7], B. Dias[4], Y. Momany[3], V. Hill[8], M. Zoccali[6,9], and C. Siqueira-Mello[1]

[1] Universidade de São Paulo, IAG, Rua do Matão 1226, Cidade Universitária, São Paulo 05508-900, Brazil; e-mail: barbuy@astro.iag.usp.br
[2] Dipartimento di Fisica e Astronomia, Università di Padova, I-35122 Padova, Italy
[3] INAF-Osservatorio Astronomico di Padova, Vicolo dell'Osservatorio 5, I-35122 Padova, Italy
[4] European Southern Observatory, Alonso de Cordova 3107, Santiago, Chile
[5] Universidade Federal do Rio Grande do Sul, Departamento de Astronomia, CP 15051, Porto Alegre 91501-970, Brazil
[6] Millenium Institute of Astrophysics, Av. Vicuña Mackenna 4860, Macul, Santiago, Chile
[7] Departamento de Ciencias Fisicas, Universidad Andres Bello, Republica 220, Santiago, Chile
[8] Laboratoire Lagrange (UMR7293), Université de Nice Sophia Antipolis, CNRS, Observatoire de la Côte dAzur, CS 34229, F-06304 Nice cedex 4, France
[9] Pontificia Universidad Catolica de Chile, Instituto de Astrofisica, Casilla 306, Santiago 22, Chile

Received; accepted

ABSTRACT

Context. The globular cluster HP 1 is projected at only 3.°33 from the Galactic center. Together with its distance, this makes it one of the most central globular clusters in the Milky Way. It has a blue horizontal branch (BHB) and a metallicity of [Fe/H]≈ −1.0. This means that it probably is one of the oldest objects in the Galaxy. Abundance ratios can reveal the nucleosynthesis pattern of the first stars as well as the early chemical enrichment and early formation of stellar populations.
Aims. High-resolution spectra obtained for six stars were analyzed to derive the abundances of the light elements C, N, O, Na, and Al, the alpha-elements Mg, Si, Ca, and Ti, and the heavy elements Sr, Y , Zr, Ba, La, and Eu.
Methods. High-resolution spectra of six red giants that are confirmed members of the bulge globular cluster HP 1 were obtained with the 8m VLT UT2-Kueyen telescope with the UVES spectrograph in FLAMES-UVES configuration. The spectroscopic parameter derivation was based on the excitation and ionization equilibrium of Fe I and Fe II.
Results. We confirm a mean metallicity of [Fe/H] = −1.06 ± 0.10, by adding the two stars that were previously analyzed in HP 1. The alpha-elements O and Mg are enhanced by about +0.3 ≲ [O,Mg/Fe] ≲ +0.5 dex, Si is moderately enhanced with +0.15 ≲ [Si/Fe] ≲ +0.35 dex, while Ca and Ti show lower values of −0.04 ≲ [Ca,Ti/Fe] ≲ +0.28 dex. The r-element Eu is also enhanced with [Eu/Fe]≈ +0.4, which together with O and Mg is indicative of early enrichment by type II supernovae. Na and Al are low, but it is unclear if Na-O are anticorrelated. The heavy elements are moderately enhanced, with −0.20 < [La/Fe] < +0.43 dex and 0.0 < [Ba/Fe] < +0.75 dex, which is compatible with r-process formation. The spread in Y, Zr, Ba, and La abundances, on the other hand, appears to be compatible with the spinstar scenario or other additional mechanisms such as the weak r-process.
Conclusions.

Key words. Galaxy: Bulge - Globular Clusters: HP 1 - Stars: Abundances, Atmospheres

1. Introduction

The globular cluster HP 1 is located at 3.°33 and 1.8 kpc from the Galactic center. This is in the inner bulge volume, and the cluster lies among the globular clusters that are closest to the Galactic center. A metallicity of [Fe/H] ∼ −1.0 was deduced from its color-magnitude diagram (CMD) by Ortolani et al. (1997, 2011). High-resolution spectroscopy of two stars performed by Barbuy et al. (2006) resulted in [Fe/H]=−1.0±0.2, and low-resolution spectroscopy of eight red giants by Dias et al. (2016) yielded a mean of [Fe/H]=−1.17±0.07. Metallicities like this are at the lower end of the metal-poor stellar population in the metallicity distribution function (MDF) of bulge stars by Zoccali et al. (2008), Hill et al. (2011) and Rojas-Arriagada et al. (2014). A lower metallicity end at [Fe/H]∼-1.0 is due to the fast chemical enrichment in the Galactic bulge as modeled for example by Cescutti et al. (2008, A&A, 491, 401). There are traces of a very metal-poor population in the bulge,

Send offprint requests to: B. Barbuy

⋆ Observations collected at the European Southern Observatory, Paranal, Chile (ESO), under programs 93.D-0124A, and 65.L-0340A

such as those found by García-Perez et al. (2013) and Howes et al. (2014, 2015). These stars are very interesting, but most of them are located in the outer bulge and might more probably be halo stars. The main fact is that the bulk of the bulge stars show a lower end at [Fe/H] ~ -1.0. A metallicity of [Fe/H] ~ -1.0 could correspond to the population C or D as defined by Ness et al. (2013a) in an MDF of a large sample of bulge stars. For a latitude b=-5° , Ness et al. found a mean [Fe/H]=-0.66 for population C stars and identified it with the thick-disk population; their population D has a mean [Fe/H]=-1.16 and was identified by them as a metal-weak thick-disk population. It is not clear whether HP 1 fits into these categories.

The following evidence shows that there may be a stellar population peak at [Fe/H] ~ -1.0 in the bulge: a) The metallicity distribution of bulge globular clusters was shown to have two peaks at [Fe/H] ≈ -0.5 and [Fe/H] ≈ -1.0 (Bica et al. 2016), where a list of known bulge clusters was selected. This had already been pointed out in Barbuy et al. (2006, 2007, 2009) and Rossi et al. (2015). b) Another piece of evidence that stars of this metallicity are very old and are characteristic of the old Galactic bulge are the findings by Walker & Terndrup (1991), who showed that RR Lyrae in the bulge show a metallicity peak at [Fe/H] ≈ -1.0 (see also Lee 1992). Based on the MACHO survey, Kunder & Chaboyer (2008) determined a mean [Fe/H]=-1.25, with a broad metallicity distribution. Dékány et al. (2013) used the VISTA Variables in the Via Lactea (VVV) survey and obtained a spheroidal and centrally concentrated distribution, with a slight elongation in its center. Using OGLE-III data, Pietrukowicz et al. (2012) derived [Fe/H]=-1.02±0.18, with a barred distribution toward the central parts of the Galaxy. From OGLE-IV Pietrukowicz et al. (2015) obtained a mean [Fe/H]=-1.025±0.25 and a triaxial ellipsoid shape. The outer bulge studied with 10^3 VVV RR Lyrae by Gran et al. (2015) shows a centrally concentrated spheroidal distribution. c) More recently, Schultheis et al. (2015) found a peak of bulge field stars at [Fe/H] ~ -1.0 that was enhanced in alpha-elements. d) Schiavon et al. (2016, in preparation) identified a sample of nitrogen-rich stars that also show metallicities of [Fe/H] ~ -1.0.

The triaxial ellipsoid shape as well as a cylindrical rotation as found in the bulge radial velocity assay (BRAVA) by Kunder et al. (2012) are expected from the dynamical evolution of an initially small classical bulge and a bar formed later in the disk (Saha et al. 2012). Therefore either a spheroidal or triaxial shape would be consistent with an initially small classical bulge.

In summary, the moderately metal-poor globular clusters in the inner Galactic bulge might be relics of an early generation of long-lived stars formed in the proto-Galaxy. For this reason we have been pursuing the study of these clusters based on spectroscopy (Barbuy et al. 2006, 2007, 2009, 2014), as well as photometry and color-magnitude diagrams (CMDs) corrected for proper motion, as can be found in Ortolani et al. (2011) and Rossi et al. (2015).

In the present work we carry out a detailed analysis with high spectral resolution of six stars of the globular cluster HP 1. This cluster has a blue horizontal branch (BHB) combined with a metallicity of [Fe/H]~ -1.0, which indicates that it is very old. Ortolani et al. (2011) derived the age by plotting HP 1 in the diagram of Fig. 17 by Dotter et al. (2010). From this, they computed an age difference of about 1 Gyr for HP 1 compared to their sample of halo clusters with ∼12.7 Gyr. This means that HP 1 is about 13.7 Gyr old and appears to be one of the oldest globular clusters in the Galaxy.

The cluster HP 1 is located at J2000 $\alpha = 17^h31^m05.2^s$, $\delta = -29°58'54''$, with Galactic coordinates l = $-2.°58$, b = $+2.°12$.

The globular cluster HP 1 was discovered at the Observatoire de Haute Provence by Dufay et al. (1954). It was first studied through CMDs by Ortolani et al. (1997) by means of V, I colors. Davidge (2000) studied individual stars in the J, H, K, and CO filters and estimated [Fe/H]=−1.6 for HP 1. Ortolani et al. (2011) used J, H, and K with the multiconjugate adaptive optics demonstrator (MAD) at the VLT, applying a proper motion decontamination procedure, making use of the time difference between the NTT observations from 1994 and the VLT/MAD observations in 2008. This allowed producing decontaminated CMDs and computing the orbit of HP 1 in the Galaxy. The CMD proper motion cleaning greatly optimizes the selection of member stars. Ortolani et al. (2011) showed that HP 1 remains confined within the bulge and/or bar. Minniti (1995) employed medium-resolution infrared spectroscopy and measured indices in six stars of HP 1. They obtained a metallicity of [Fe/H]=−0.56 and a radial velocity of 60 km.s^{-1}. Stephens et al. (2004) used medium-resolution infrared spectra of six stars in HP 1 and derived a metallicity of [Fe/H]=−1.30. Two stars of HP 1 were observed at high spectral resolution with UVES and were analyzed spectroscopically (Barbuy et al. 2006), program 65.L-0340 (PI: D. Minniti). To provide the most accurate information on the abundance pattern and kinematics of the metal-poor bulge globular clusters, we analyze a more significant number of stars in HP 1 to better identify the characteristics of the probably oldest stellar population in the Galaxy.

In this work we present a detailed abundance analysis using data from the FLAMES-UVES spectrograph at the VLT with a resolution R $\sim$ 45,000 and a signal-to-noise ratio S/N > 200 for all sample stars. The MARCS model atmospheres are employed (Gustafsson et al. 2008).

The observations are described in Sect. 2. The effective temperature of the photometric stellar parameters and the gravity are derived in Sect. 3. Spectroscopic parameters are derived in Sect. 4 and abundance ratios are computed in Sect. 5. A discussion is presented in Sect. 6 and conclusions are drawn in Sect. 7.

2. Observations

The sample member stars of HP 1 were selected from data corrected for the proper motion that were reported in Ortolani et al. (2011). Figure 1 shows a JHK_s-combined image of HP 1 from the Vista Variables in the Via Lactea VVV survey (Saito et al. 2012)[1]. The location of the six sample stars together with the two stars previously analyzed in Barbuy et al. (2006) are shown

[1] http://horus.roe.ac.uk/vsa/

in Fig. 2, with the observed field in a z-color image from the VVV survey.

The spectra of individual stars of HP 1 were obtained at the VLT using the UVES spectrograph (Dekker et al. 2000) in FLAMES-UVES mode. The red arm (5800−6800 Å) has the ESO CCD # 20 chip, an MIT backside illuminated, with a size of 4096 x 2048 pixels, and a pixel size of 15 x 15 μm. The blue arm (4800−5800 Å) uses the ESO Marlene EEV CCD#44 chip, backside illuminated, with a size of 4102 x 2048 pixels, and a pixel size of 15 x 15μm. The UVES standard setup 580 yields a resolution R $\sim$ 45,000 for a slit width of 1 arcsec. The pixel scale is 0.0147 Å/pix, with $\sim$ 7.5 pixels per resolution element at 6000 Å. The data were reduced using the UVES pipeline within the ESO/Reflex software (Ballester et al. 2000; Modigliani et al. 2004). The log of the 2014 observations is given in Table 1. The spectra were flat fielded, optimally extracted, and wavelength calibrated with the FLAMES-UVES pipeline. Spectra extracted from different frames were then co-added, taking into account the radial velocities reported in Table 2. The present UVES observations centered on 5800 Å yield a spectral coverage of 4800 < λ < 6800 Å, with a gap at 5708−5825 Å.

We measured the radial velocities of each run using the IRAF FXCOR cross-correlation method, as reported in Table 2. The mean errors reported from the IRAF routine are 1.52 km s^{-1}. These values are clearly higher than jitter variations, which are estimated to be around 0.1 km s^{-1} (e.g., Hekker et al. 2008).

The present mean heliocentric radial velocity v_r^{hel} = +40.0 ± 0.5 km s^{-1} agrees very well with the value of +45.8 km s^{-1} derived from two stars in Barbuy et al. (2006). These are very low radial velocities, which combined with the low proper motions (Ortolani et al. (2011) support the possibility of a confinement in the bulge.

Figure 3 shows the V, I CMD of HP 1 and the location of the program stars on the red giant branch.

Table 2. Radial velocities of the UVES sample stars in each of the seven exposure runs, corresponding heliocentric radial velocities, and mean heliocentric radial velocity.

Target	v_r^{obs} km s^{-1}	$v_r^{hel.}$ km s^{-1}	Target	v_r^{obs} km s^{-1}	$v_r^{hel.}$ km s^{-1}
2115 1	+37.024	+41.004	2461 1	+36.430	+40.41
2115 2	+45.313	+41.143	2461 2	+44.920	+40.75
2115 3	+57.650	+41.140	2461 3	+57.695	+41.185
2115 4	+60.847	+40.797	2461 4	+61.178	+41.128
2115 5	+65.612	+40.812	2461 5	+65.902	+41.102
2115 6	+65.699	+40.799	2461 6	+65.995	+41.095
2115 7	+65.819	+40.839	2461 7	+66.137	+41.157
Mean	—	+41.006	Mean	—	+41.048
2939 1	+41.756	+45.736	3514 1	+31.695	+35.675
2939 2	+50.289	+46.119	3514 2	+39.904	+35.734
2939 3	+62.512	+46.002	3514 3	+52.524	+36.014
2939 4	+66.057	+46.007	3514 4	+55.573	+35.523
2939 5	+70.718	+45.918	3514 5	+59.992	+35.192
2939 6	+70.859	+45.959	3514 6	+60.104	+35.204
2939 7	+70.974	+45.994	3514 7	+60.168	+35.188
Mean		+46.035	Mean	—	+35.577
5037 1	+37.355	+41.335	5485 1	+30.851	+34.831
5037 2	+45.627	+41.457	5485 2	+38.234	+34.064
5037 3	+58.229	+41.719	5485 3	+50.745	+34.235
5037 4	+61.994	+41.994	5485 4	+54.665	+34.615
5037 5	+66.700	+41.900	5485 5	+59.565	+34.765
5037 6	+66.684	+41.784	5485 6	+59.782	+34.882
5037 7	+66.978	+41.998	5485 7	+59.832	+34.852
Mean		+41.807	Mean	—	+34.679

3. Photometric stellar parameters

3.1. Temperatures

The selected stars, their ID and 2MASS designations, coordinates, V, I magnitudes from Ortolani et al. (1997), and the 2MASS JHK$_s$ (Skrutskie et al. 2006)[2] and VVV JHK$_s$ magnitudes (Saito et al. 2012) are listed in Table 3. These magnitudes and colors were used to derive initial estimates of the effective temperature and gravity, which were fine-tuned with spectroscopic data using the Fe I and Fe II lines (see Sect. 4).

For star 2461, the identification in the VVV images seems to indicate a blend of at least three stars, as can be seen in Fig. 4. The VVV reductions were made in aperture photometry, which does not yield reliable magnitudes in this case. Only PSF photometry, which is being carried out by the VVV group, will allow distinguishing such cases. For the spectroscopy, the size of 1 arcsec of the fiber does allow observing the correct star.

The reddening value of $E(B-V)$ = 1.19 was derived from V, I CMDs by Ortolani et al. (1997). Barbuy et al. (1998) adopted $E(B-V)$ = 1.21 by using a slightly different R_V value. Barbuy et al. (2006) reported previous literature extinction values, and based on a reanalysis of CMD data, adopted $E(B-V)$ = 1.12. Ortolani et al. (2011) adopted $E(V-K)$ = 3.33, which translates into $E(B-V)$ = 1.21 using E($V-K$)/E($B-V$) = 2.744 (Rieke & Lebofsky 1985); the use of a different reddening law does not affect the result much. In the present work we adopted $E(B-V)$ = 1.12, following Barbuy et al. (2006).

Effective temperatures were derived from $V-I$, $V-K$, and $J-K$ using the color-temperature calibrations of Alonso et al. (1999, hereafter AAM99). These relations are similar to those by Ramirez & Meléndez (2005), as shown in their Fig. 11. The advantage of using the calibrations of Alonso et al. is that the bolometric corrections can be calculated, despite the disadvantage of having to translate Cousins to Johnson I, and 2MASS to TCS JHK colors. To translate $V-I$ from the Cousins to the Johnson system, we adopted $(V-I)_C$=0.778$(V-I)_J$ (Bessell 1979). The J, H, K_S 2MASS magnitudes and colors were translated from the 2MASS system to CIT (California Institute of Technology), and from this to TCS (Telescopio Carlos Sánchez), using the relations from Carpenter (2001) and Alonso et al. (1998). The VVV JHK_s colors were translated into the 2MASS JHK_s system, using relations reported by Soto

[2] http://ipac.caltech.edu/2mass/releases/allsky/

Table 1. Log of the spectroscopic observations: dates, Julian dates, exposure times, airmass, seeing, and run number.

Date	UT	HJD	exp (s)	Airmass	Seeing (″)	run
07.06.14	04:33:15	2456815.69535	3000	1.007-1.013	0.72-0.84	1
24.06.14	01:55:50	2456832.58620	2700	1.083-1.026	0.47-0.73	2
20.07.14	05:13:40	2456858.72267	2700	1.329-1.591	0.52-0.53	3
30.07.14	01:26:09	2456868.56407	2700	1.004-1.023	0.83-0.75	4
14.08.14	01:00:33	2456883.54517	2750	1.010-1.047	0.71-0.69	5
14.08.14	01:58:18	2456883.54517	2750	1.048-1.126	0.64-0.72	6
14.08.14	02:45:54	2456883.61832	2750	1.129-1.264	0.77-1.00	7

Table 3. Identifications, coordinates, V, I magnitudes from Ortolani et al. (1997), and JHK_s magnitudes from the 2MASS and VVV surveys. The two stars analyzed in Barbuy et al. (2006) are also listed. [a]: identification of star 2461 in VVV may be a blend of stars.

ID no.	2MASS ID	α_{2000}	δ_{2000}	V	I	J	H	K_s	J_{VVV}	H_{VVV}	K_{VVV}
2115	— - —	17:31:05.420	−29:59:20.71	17.070	14.281	—	—	—	—	—	—
2461	17310822-2959108	17:31:08.22	−29:59:10.85	17.115	14.628	—	—	—	12.066[a]	10.249[a]	10.959[a]
2939	17310729-2959021	17:31:07.31	−29:59:02.30	17.131	14.394	11.901	10.869	10.595	—	—	—
3514	17310273-2958544	17:31:02.74	−29:58:54.74	17.327	14.721	12.447	11.574	11.212	—	11.248	11.378
5037	17310347-2958259	17:31:03.48	−29:58:26.04	17.101	14.487	12.302	11.303	10.994	12.287	11.502	11.115
5485	17310817-2958147	17:31:08.19	−29:58:14.81	17.116	14.710	12.761	11.965	11.364	12.737	11.989	11.729
hp1-2	17310585-2958354	17:31:05.852	−29:58:35.5	16.982	14.332	12.21	11.268	10.969	12.1527	11.4164	11.0541
hp1-3	17310587-2959180	17:31:05.872	−29:59:18.1	17.003	14.358	12.167	11.146	10.828	12.1220	10.9702	10.9119

Table 4. Photometric stellar parameters derived using the calibrations by Alonso et al. (1999) for $V-I$, $V-K$, $J-K$, bolometric corrections computed by adopting the V, I derived temperature, bolometric magnitudes, and corresponding gravity log g, and final spectroscopic parameters. A reddening of $E(B-V) = 1.12$ is assumed. For each star the last columns give the spectroscopic parameters from UVES spectra (present work).

	Photometric parameters								Spectroscopic parameters							
star	T_{V-I}	T_{V-K}	T_{J-K}	T_{V-K}	T_{J-K}	BC_V	M_{bol}	log g	T_{eff}	BC_V	log g	log g	[FeI/H]	[FeII/H]	[Fe/H]	v_t
		2MASS		VVV												
	(K)	(K)	(K)	(K)	(K)				(K)							km s^{-1}
2115	4196.6	—	—	—	—	−0.702	−0.18	1.95	4530	−0.457	1.99	2.00	−0.98	−1.02	−1.00	1.45
2461	4735.2	—	—	4217.9	4506.5	−0.368	−0.14	2.04	4780	−0.323	2.04	2.05	−1.13	−1.09	−1.11	1.90
2939	4274.4	4025.1	4423.3	—	—	−0.638	−0.12	1.98	4525	−0.440	2.01	2.00	−1.07	−1.07	−1.07	1.55
3514	4496.6	4249.4	4624.0	4855.9	—	−0.487	0.08	2.09	4590	−0.349	2.06	2.00	−1.18	−1.19	−1.18	1.90
5037	4481.9	4254.3	4418.0	4324.0	4576.4	−0.496	−0.15	1.99	4570	−0.429	2.05	2.15	−0.98	−1.03	−1.0	1.20
5485	4920.4	4499.6	4197.0	4812.7	5152.4	−0.298	0.14	2.08	4920	−0.282	2.09	2.07	−1.18	−1.18	−1.18	1.80

et al. (2013). The derived photometric effective temperatures are listed in Table 4.

3.2. Gravities

The gravity values were computed using the classical formula

$$\log g_* = 4.44 + 4 \log \frac{T_*}{T_\odot} + 0.4(M_{\rm bol*} - M_{\rm bol\odot}) + \log \frac{M_*}{M_\odot}$$

We adopted $T_\odot = 5770$ K and $M_{bol\odot} = 4.75$ for the Sun and $M_* = 0.85\ M_\odot$ for the red giant branch (RGB) stars. For HP 1

we assumed a distance modulus of $(m-M)_0 = 14.15$ (Ortolani et al. 1997, 2011), and the gravities were computed and are reported in Table 4. Bolometric corrections were computed with formulae by AAM99. The photometric gravity values were computed assuming the bolometric corrections from the temperature T(V-I) values (Col. 9), and also with the spectroscopic temperature values (Col. 11). The final spectroscopic gravities, described in the next section, are given in Col. 12 of Table 4, and are compatible with the photometric gravities.

4. Spectroscopic stellar parameters

The equivalent widths (EW) were measured using the automatic code DAOSPEC, developed by Stetson & Pancino (2008). We also measured EWs line by line using IRAF for a few lines, in particular for Fe II . The EWs measured for the Fe I and Fe II lines are reported in Table A.1. We limited EWs to 20 < EW(mÅ) < 99 to avoid on one hand, too weak lines that are affected by the continuum level choice, in particular when using software such as DAOSPEC, and on the other hand, the saturated lines that are less sensitive to abundance variations.

In Fig. 5 we show the computed Fe II lines compared with the observed spectra. Given the blends in lines Fe II 6084.11 and 6456.39 Å, these lines were not used.

In the line list given in Table A.1, literature oscillator strengths for Fe I from NIST[3] and VALD3[4] databases (Martin et al. 2002; Piskunov et al. 1995) are reported. We also give the adopted values, where we have given preference to NIST over VALD. For Fe II we report the log gf values from Fuhr & Wiese (2006) and Meléndez & Barbuy (2009) in Table A.1. We adopted the latter values.

Photospheric 1D models for the sample giants were extracted from the MARCS model atmosphere grid (Gustafsson et al. 2008). We adopted the spherical and mildly CN-cycled set ([C/Fe]= −0.13, [N/Fe]= +0.31). This choice is due to the well-known mixing that occurs along the RGB, which transforms C into N. These models consider [α/Fe]=+0.20 for [Fe/H]=-0.50 and [α/Fe]=+0.40 for [Fe/H]≤ −1.00. The LTE abundance analysis and the spectrum synthesis calculations were performed using the code described in Barbuy et al. (2003) and Coelho et al. (2005). An Fe abundance of ϵ(Fe)= 7.50 (Grevesse & Sauval 1998) was adopted. Molecular lines of MgH ($A^2\Pi$-$X^2\Sigma$), CN ($A^2\Pi$-$X^2\Sigma$), C_2 Swan ($A^3\Pi$-$X^3\Pi$), TiO ($A^3\Phi$-$X^3\Delta$) γ and TiO ($B^3\Pi$-$X^3\Delta$) γ' systems are taken into account.

The stellar parameters were derived by initially adopting the photometric effective temperature and gravity, and then by further constraining the temperature by imposing excitation equilibrium for Fe I lines. Fe I and Fe II lines allowed deriving gravities by imposing ionization equilibrium. Microturbulence velocities v_t were determined by canceling the trend of Fe I abundance vs. equivalent width.

The final spectroscopic parameters $T_{\rm eff}$, log g, [Fe I/H], [Fe II/H], [Fe/H], and v_t values are reported in the last columns of Table 4. An example of excitation and ionization equilibria using Fe I and Fe II lines is shown in Fig. 6 for star HP1-2939.

[3] http://physics.nist.gov/PhysRefData/ASD/lines_form.html
[4] http://vald.astro.univie.ac.at/ vald3/php/vald.php

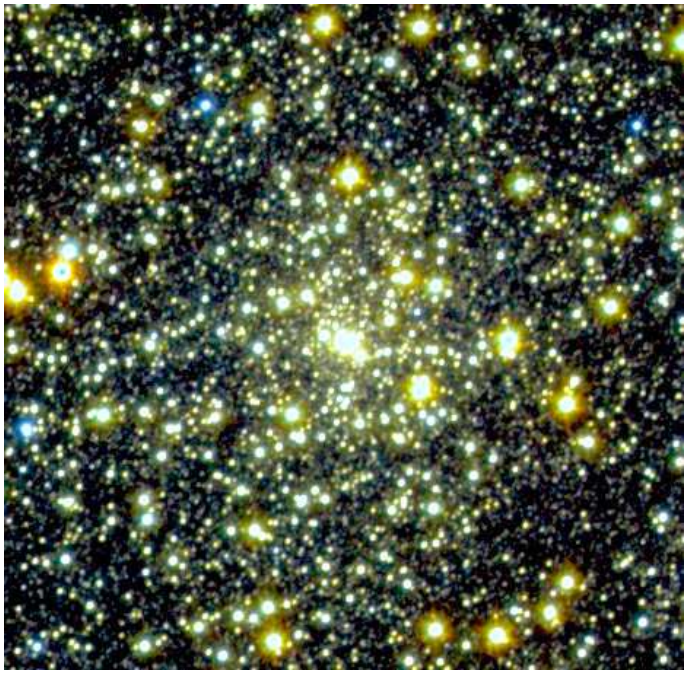

Fig. 1. HP 1 JHK_s-combined colour image from the VVV survey. The image has size of 2×2 arcmin^2. North is at 45° anticlockwise.

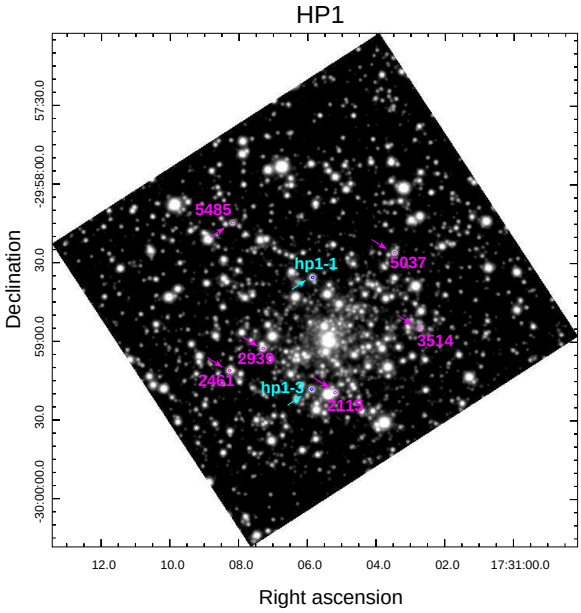

Fig. 2. z image from the VVV survey, indicating the location of the sample stars.

5. Abundance ratios

Abundance ratios were obtained by means of line-by-line spectrum synthesis calculations compared to the observed spectra for the line lists given in Tables 5, 6, 7, and 8. The fits were made by eye using a series of calculations for different

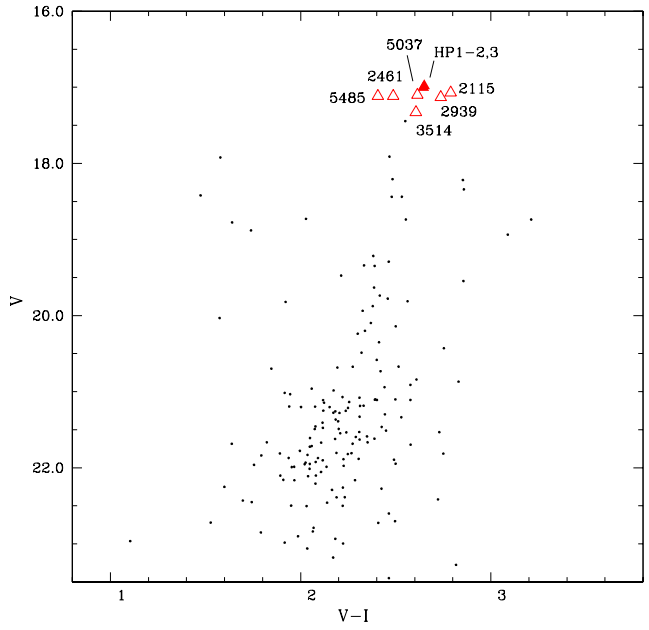

Fig. 3. V, I CMD of HP 1 based on data from Ortolani et al. (1997), with the V, V−I of the sample stars indicated.

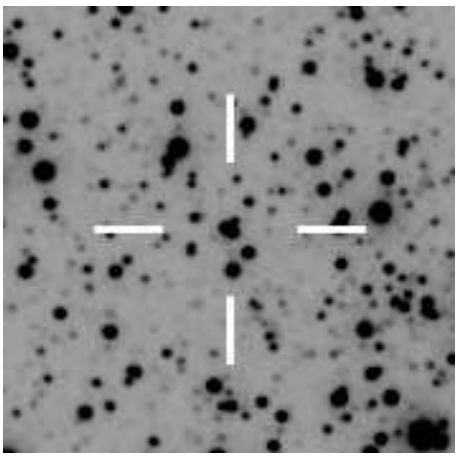

Fig. 4. Image of star 2461 in the VVV survey, indicating a blend of stars. Extraction of ∼ 20 arcsec. North is 45○ anti-clockwise.

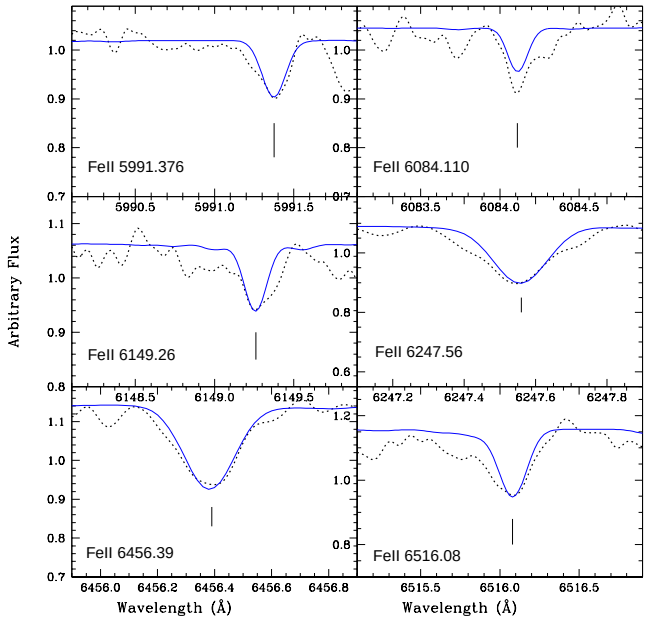

Fig. 5. FeII lines for star 5037. Dotted lines: observed spectra. Blue solid lines: synthetic spectra.

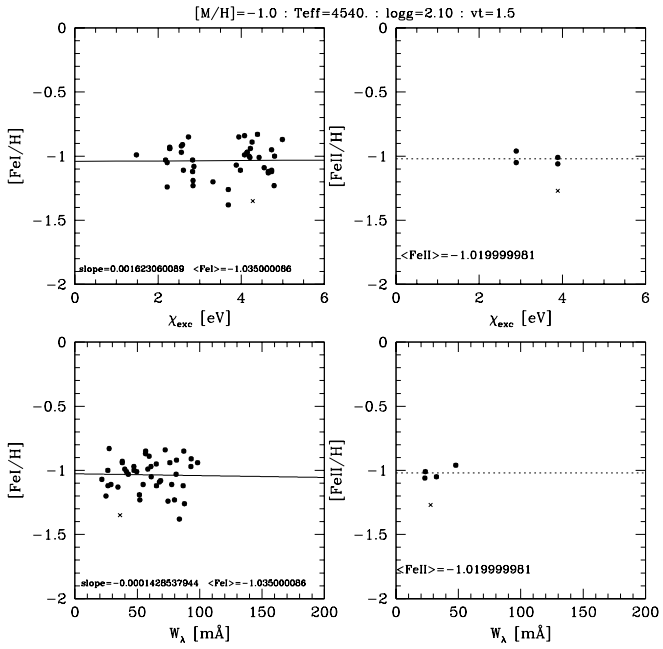

Fig. 6. Excitation and ionization equilibria of Fe I and Fe II lines for star 2939.

abundances and verifying the continua over 20 Å. We then zoomed and fine-tuned them locally. The solar abundances were adopted from Grevesse et al. (1998), which are close to the latest values by Asplund et al. (2009), Grevesse et al. (2014) or Lodders (2009). For oxygen we adopted ϵ(O)= 8.77 following Allende Prieto et al. (2001) for 1D model atmospheres, which is very close to the value of ϵ(O)= 8.76 recommended from 3D models by Steffen et al. (2015).

5.1. Carbon, nitrogen, and oxygen

The carbon abundances were estimated from the C_2(0,1) bandhead at 5635.3 Å. The list of laboratory C_2 lines (Phillips & Davis 1968) was reported in Barbuy et al. (2014). Because the feature is weak in these metal-poor stars, we adopted [C/Fe]= 0.0 and just checked that this was a suitable upper limit. The nitrogen abundances were measured using the CN (5,1) 6332.18

Table 6. Abundances of light elements Na, Mg, Al.

species	λ (Å)	χ_{ex}(eV)	log gf	2115	2461	2939	3514	5037	5485	HP1-2	HP1-3
NaI	5682.633	2.102439	−0.706	−0.15	-0.30	−0.30	+0.00	−0.10	−0.30	+0.00	−0.20
NaI	5688.194	2.104571	−1.400	+0.20	-0.30	-0.15	-0.20	−0.10	−0.30	−0.10	−0.20
NaI	5688.205	2.104571	−0.45	+0.20	-0.30	-0.15	-0.20	−0.10	−0.30	−0.10	−0.20
NaI	6154.230	2.102439	−1.56	0.05	−0.10	−0.15	−0.15:	+0.20	−0.30	−0.30	+0.05
NaI	6160.753	2.104571	−1.26	+0.25	−0.15	−0.15	+0.10	+0.30	+0.00	−0.30	—
AlI	6696.185	4.021753	−1.576	−0.1	+0.0	+0.1	+0.00	+0.20	+0.20:	-0.25	+0.15
AlI	6696.788	4.021919	−1.421	—	—	—	—	—	—	—	—
AlI	6698.673	3.142933	−1.647	−0.10	+0.10	0.00	+0.10	+0.20	+0.20	−0.30	+0.20
MgI	6318.720	5.108171	−2.10	+0.30	+0.30	+0.50	+0.40	+0.40	+0.40	+0.15	+0.35
MgI	6319.242	5.108171	−2.36	+0.30	+0.40	+0.30	+0.30	+0.20	+0.40	—	+0.30

Table 5. Carbon, nitrogen, and oxygen abundances derived from C_2 (0,1), CN (5,1), and [OI] lines.

line	λ(Å)	2115	2641	2939	3514	5037	5485
C_2(0,1)	5635.5	≤+0.0	≤+0.0	≤+0.0	≤+0.0	≤+0.0	≤+0.0
CN(5,1)	6332.2	≤+0.7	≤+0.5	≤+0.5	≤+0.8	≤+0.5	≤+0.5
[OI]	6300.3	+0.4	+0.5	+0.5	+0.4	+0.35	+0.4

Å of the CN $A^2\Pi$-$X^2\Sigma$ red system. The CN feature is also weak, but can be used to estimate a reliable upper limit for the N abundance.

The forbidden oxygen [OI] 6300.311 Å line was used to derive the oxygen abundances. A check for telluric lines was carried out by overplotting the spectrum of a fast-rotation B star, and we verified that none of the stars were affected by them. The resulting C, N, and O abundances are given in Table 5, showing the essentially adopted carbon abundance of [C/Fe]∼ 0.0, the enhanced nitrogen abundances as expected in giants, and enhanced oxygen abundances of +0.35 < [O/Fe] < +0.5, typical of enrichment by SNII.

5.2. Odd-Z elements Na, Al, and alpha-elements

In Table 6 and 7 we report the line-by-line abundances of the odd-Z elements Na, Al, and the alpha-elements Mg, Si, Ca, and Ti abundances. We have inspected the abundance results as a function of effective temperature and microturbulence velocity and found no trend for any of the elements. In addition to the six sample stars, we also rederived the abundances of Na, Al and Mg for the two stars analyzed in Barbuy et al. (2006), as given in Table 6.

5.3. Heavy elements

In Table 8 we report the line-by-line derivation of abundances for lines of the neutron-capture dominant s-elements Sr, Y, Zr, La, Ba, and the r-element Eu. As in Table 6, we also rederived the abundances of heavy elements for the two stars analyzed in Barbuy et al. (2006). The hyperfine structure (HFS) for the studied lines of La II, Ba II and Eu II were taken into account, as described in Barbuy et al. (2014). The fits to the lines of Eu II 6645, Ba II 6141 and Ba II 6496 Å lines in star 2115 are shown in Fig. 8.

Fig. 7. [Na/Fe] vs. [O/Fe] for the sample stars compared with stars of NGC 6121. Symbols: present work: green filled squares: the 6 HP 1 stars with [Fe/H] = −1.0 ± 0.05; open green squares: the 2 HP 1 stars with [Fe/H]=-1.18, compared with blue filled triangles: stars of NGC 6121.

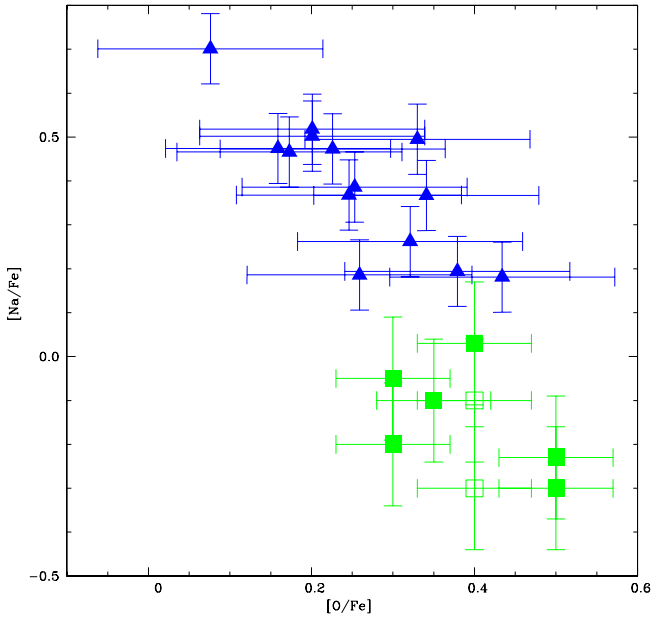

5.4. Errors

The errors due to uncertainties in spectroscopic parameters are given in Table 9, applied to the sample star HP 1: 2115. The error on the slope in the FeI *vs.* excitation potential implies an error in the temperature of ±100 K for the sample stars. An uncertainty of the order of 0.2 km s^{-1} on the microturbulence

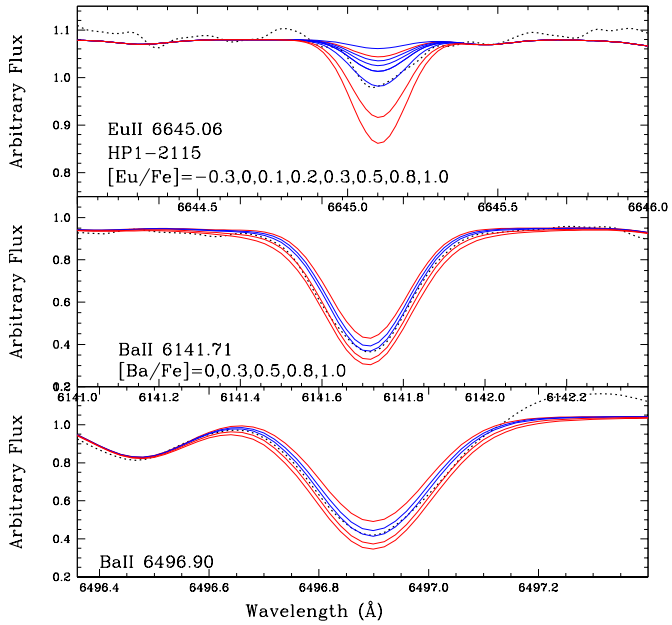

Fig. 8. Fits to the Eu II 6645, Ba II 6141 and Ba II 6496 Å lines in star 2115. The [Eu/Fe] and [Ba/Fe] values adopted for the different calculations are indicated in the panels.

velocity is estimated from the imposition of a constant value of [Fe/H] as a function of EWs. Errors based on EWs are given on FeI and FeII abundances.

The errors on the abundance ratios [X/Fe] were computed by fitting the lines with the modified atmospheric model. The error reported corresponds to the new value obtained by using the modified model atmosphere. The element abundance ratios, induced by a change of ΔTeff = +100 K, Δlog g= +0.2, Δv_t = 0.2 km s^{-1}, and a total error estimate, are given in Table 9. These errors are overestimated because the stellar parameters are covariant. The correlation matrix is difficult to estimate, however, and would add other error sources, so that we preferred the quadratic sum of the diagonal terms as reliable.

Additionally, an uncertainty of about 0.8 mÅ in the EWs of the Fe lines was estimated with the formula of (Cayrel 1988; Cayrel 2004). With a mean FWHM = 12.5 pixels, or 0.184 Å, a CCD pixel size of 15 μm, or δx = 0.0147 Å in the spectra, and assuming a mean S/N=100, we obtain an error ΔEW ∼ 0.8 mÅ.

We derived abundances uniquely from fitting synthetic spectra, such that we need to take the uncertainty in the continuum placement into account. We estimate an error of 0.1dex for the weak and strong lines and 0.05 dex for medium lines. This is included in Table 9.

6. Discussion

In Table 10 we report the mean abundances for each star and for each element, and in the last line we report the radial velocities.

Table 9. Abundance uncertainties for star 2115 for uncertainties of ΔT_{eff} = +100 K, Δlog g= +0.2, Δv_t = 0.2 km s^{-1}, an assumed error in EWs or continuum placement, and the corresponding total error. The errors correspond to the difference in abundance obtained with the modified parameters.

Abundance	ΔT 100 K	Δlog g 0.2 dex	Δv_t 0.2 kms^{-1}	EW	$(\sum x^2)^{1/2}$
(1)	(2)	(3)	(4)	(5)	
[FeI/H]	+0.06	+0.03	−0.07	0.02	0.10
[FeII/H]	−0.12	+0.11	−0.03	0.02	0.17
[N/Fe]	−0.05	+0.00	+0.00	0.10	0.11
[O/Fe]	+0.00	−0.05	+0.00	0.05	0.07
[NaI/Fe]	+0.10	+0.00	−0.01	0.10	0.14
[Al/Fe]	+0.05	+0.00	+0.00	0.10	0.11
[MgI/Fe]	+0.03	+0.00	+0.00	0.10	0.10
[SiI/Fe]	+0.00	+0.02	−0.02	0.05	0.06
[CaI/Fe]	+0.10	+0.00	−0.05	0.05	0.12
[TiI/Fe]	+0.10	+0.00	−0.03	0.05	0.12
[TiII/Fe]	−0.10	+0.08	−0.01	0.05	0.14
[SrI/Fe]	−0.15	+0.00	+0.00	0.20	0.25
[YI/Fe]	−0.15	+0.00	+0.00	0.10	0.18
[YII/Fe]	+0.02	−0.15	+0.00	0.10	0.18
[ZrI/Fe]	−0.20	+0.00	+0.00	0.10	0.22
[BaII/Fe]	+0.02	+0.02	−0.20	0.10	0.23
[LaII/Fe]	+0.00	+0.03	+0.00	0.10	0.10
[EuII/Fe]	+0.00	+0.03	+0.00	0.10	0.10

6.1. Two stellar populations?

We derived a mean metallicity of [Fe/H]= −1.06 ± 0.15 by adding the two stars previously analyzed in HP 1 by Barbuy et al. (2006).

Two stars, 3514 and 5485, show a slightly lower metallicity of [Fe/H]= −1.18 and, possibly not by coincidence, they also show radial velocities of v_r^{hel} = +35.6 and +34.7 km s^{-1}, respectively, which is lower than the radial velocities of the other six stars, whose values lie in the range −41.0 < v_r^{hel} < −47.0 km s^{-1}. Their radial velocities are compatible with being members within the uncertainties. If these two stars correspond to an earlier stellar generation in the cluster, then we might have a first stellar generation with [Fe/H]=−1.18 and a second generation with a mean metallicity of [Fe/H]= −1.02 ± 0.05, as found for the other six stars.

The membership of these two lower velocity stars is another question. Recent work by Bellini et al. (2015) for NGC 2808 has shown differences in radial velocities between two stellar populations in a cluster. Malavolta et al. (2015) studied M4, showing that it has a dispersion of 4 km s^{-1}. HP 1 is probably subject to tidal effects that lead to possible perturbations or even disruption. The two low-velocity stars might become unbound from the cluster, given their difference in velocites of Δv_r^{hel}=−10 km s^{-1} .

6.2. Odd-Z elements and Na-O anticorrelation

Na and Al tend to be underabundant in HP 1. This may be due to internal nucleosynthesis (Gratton et al. 2012). In particular, a Na-O anticorrelation due to the Ne-Na cycle of proton capture reactions was shown by Carretta et al. (2009) to be confirmed for several globular clusters. In Fig. 7 we show the [Na/Fe] vs. [O/Fe] for 14 stars of NGC 6121 by Carretta et al. (2009), compared to the present results for HP 1. This figure points to evidence for a Na-O anticorrelation in HP 1, but with the difference with respect to NGC 6121 and most other clusters studied by Carretta et al. (2009), of Na being lower than in the other clusters. Na is originally probably underabundant in HP 1, which reinforces its peculiar pattern.

6.3. Alpha-elements

The α-element enhancements in O, Mg, and Si together with the enhancement of the r-process element Eu are indicative of a fast early enrichment by SNII. Ca and Ti are only slightly enhanced with [Ca/Fe]= +0.13 and [Ti/Fe]= +0.18 (a mean of Ti I and Ti II abundances). The difference between O, Mg, and Si on one hand and Ca and Ti on the other was also detected in other bulge samples, such as NGC 6522 (Barbuy et al. 2014). The mean values for NGC 6522 are reported for comparison purposes in Table 10.

The fact that [O,Mg,Si/Fe] are higher than [Ca,Ti/Fe] does not match the results for field stars by González et al. (2011). This might be explained by the mass of supernovae type II that enriched the cluster, or else by the absence of contribution from supernovae type I.

6.4. Heavy elements

Figure 9 shows the results for Y, Zr, Ba, La, and Eu compared to other available heavy element abundance determinations in bulge stars. The Sr abundances are not very reliable because the lines used are extremely faint. We therefore did not plot this element. Literature data include a) field red giants in Plaut's field analyzed by Johnson et al. (2012), b) seven red giants in the globular cluster M62 (NGC 6266) by Yong et al. (2014), c) microlensed bulge dwarf stars analyzed by Bensby et al. (2013), d) four red giants in NGC 6522 analyzed by Barbuy et al. (2014), e) 56 bulge field red giants for which Van der Swaelmen et al. (2016) derived heavy element abundances, and f) five bulge field red giants with [Fe/H]≈ -1.0 from the sample by Ness et al. (2013a) that were analyzed by Siqueira-Mello et al. (2016).

This figure shows that [Zr/Fe], [Ba/Fe], [La/Fe], and [Eu/Fe] increase steadily with decreasing metallicity. At a metallicity of around [Fe/H]≈ -1.0, the dominantly s-elements Y, Zr, Ba, and La show an abundance spread. This behavior is compatible with expectations from massive spinstars: a spread like this is predicted from the models by Frischknecht et al. (2016, and references therein) and Meynet et al. (2015, and references therein), as discussed and shown in Chiappini et al. (2011), Chiappini (2013), and Barbuy et al. (2014).

On the other hand, the enhancements of O, Mg, and Eu, and to a lesser extent of Si, Ca, and Ti, indicate an early enrichment by supernovae type II. The small fraction of r-process production of the dominantly s-elements in the solar neighborhood might be responsible for their production at early times, as first suggested by Truran (1981). To verify the r- or s-nature of the heavy element abundances, we report the [Ba/Eu] ratios in penultimate line of Table 10.

The ratio [Ba/Eu] is indicative of the relative contribution of the s- and r-process. We find $-0.60 <$ [Ba/Eu] $< +0.25$, and $[Ba/Eu]_r \sim -0.8$ is given as typical of a pure r-process by Bisterzo et al. (2014). This means that the barium-to-europium ratio is above the line for a pure r-process and might be interpreted as due to an s-process. The s-process can be due to transfer of matter from an AGB companion or to a general AGB pollution, as recently made likely to occur in multi-population clusters (e.g. Renzini et al. 2015), or to spinstars. The spread in abundances of Y, Sr, Zr, Ba, and La at around [Fe/H]~ -1.0 is the main indicator of the contribution by spinstars (Chiappini et al. 2011). Finally, both r- and s- processes may take place, that is, massive spinstars producing s-elements may not exclude a later explosion of the supernova and the subsequent r-process. Another possible explanation would be an additional process that enhanced the lightest heavy elements at early times. Several models are proposed in the literature, such as the lighter element primary process LEPP. Travaglio et al. (2004) discussed this process for the Sun. A different LEPP mechanism was discussed by Montes et al. (2007) for metal-poor stars. A possible explanation for the LEPP is the weak r-process (Wanajo & Ishimaru 2006) or supernovae neutrino-driving winds (Arcones & Thielemann 2013). We note that different processes might be enriching in Y, Sr, and Zr at different metallicities and environments. Niu et al. (2015) proposed a unified solution. Finally, it is important to mention that, as pointed out by Roederer et al. (2010) (see his Fig. 11), there are varying degrees of enrichment of first- and second-peak elements in stars enriched by neutron capture.

7. Conclusions

We carried out a detailed analysis of six red giants of the bulge moderately metal-poor globular cluster HP 1 and added two other previously analyzed stars. A metallicity of [Fe/H]= -1.06 ± 0.15 was derived from the eight stars, and since HP 1 has a blue horizontal branch, this combination of characteristics is an indication of a very old age.

We found overabundances of the α-elements [Mg/Fe]$\approx$[O/Fe]$\approx$+0.4 and [Si/Fe]$\approx$+0.3 and lower values of [Ca/Fe]$\approx$[Ti/Fe]$\approx$+0.10. The light odd-Z elements Na and Al are low with [Na/Fe]=-0.20 and [Al/Fe]=+0.18. In particular, because of the low Na abundance, the Na-O anticorrelation is unclear. HP 1 has a relatively low mass, with absolute magnitude M_V=-6.46, therefore it is probably less prone to show this effect, as demonstrated for several clusters by Carretta et al. (2009).

The dominantly s-elements are moderately enhanced with [Ba/Fe]$\approx +0.32$ and the r-element [Eu/Fe]$\approx +0.30$. These values are very similar to the results for NGC 6522 (Barbuy et al.

Fig. 9. [Y,Zr,Ba,La,Eu/Fe] vs. [Fe/H] and [Y/Ba] vs. [Fe/H] for the sample stars compared with literature values. Symbols: blue filled squares: NGC 6522; magenta pentagons: M62; red filled triangles: bulge field dwarfs by Bensby et al. (2013); blue triangles: bulge field red giants from Rich et al. (2012); cyan triangles: Van der Swaelmen et al. (2016); yellow triangles: Siqueira-Mello et al. (2016); green filled pentagons: HP 1 from the present work.

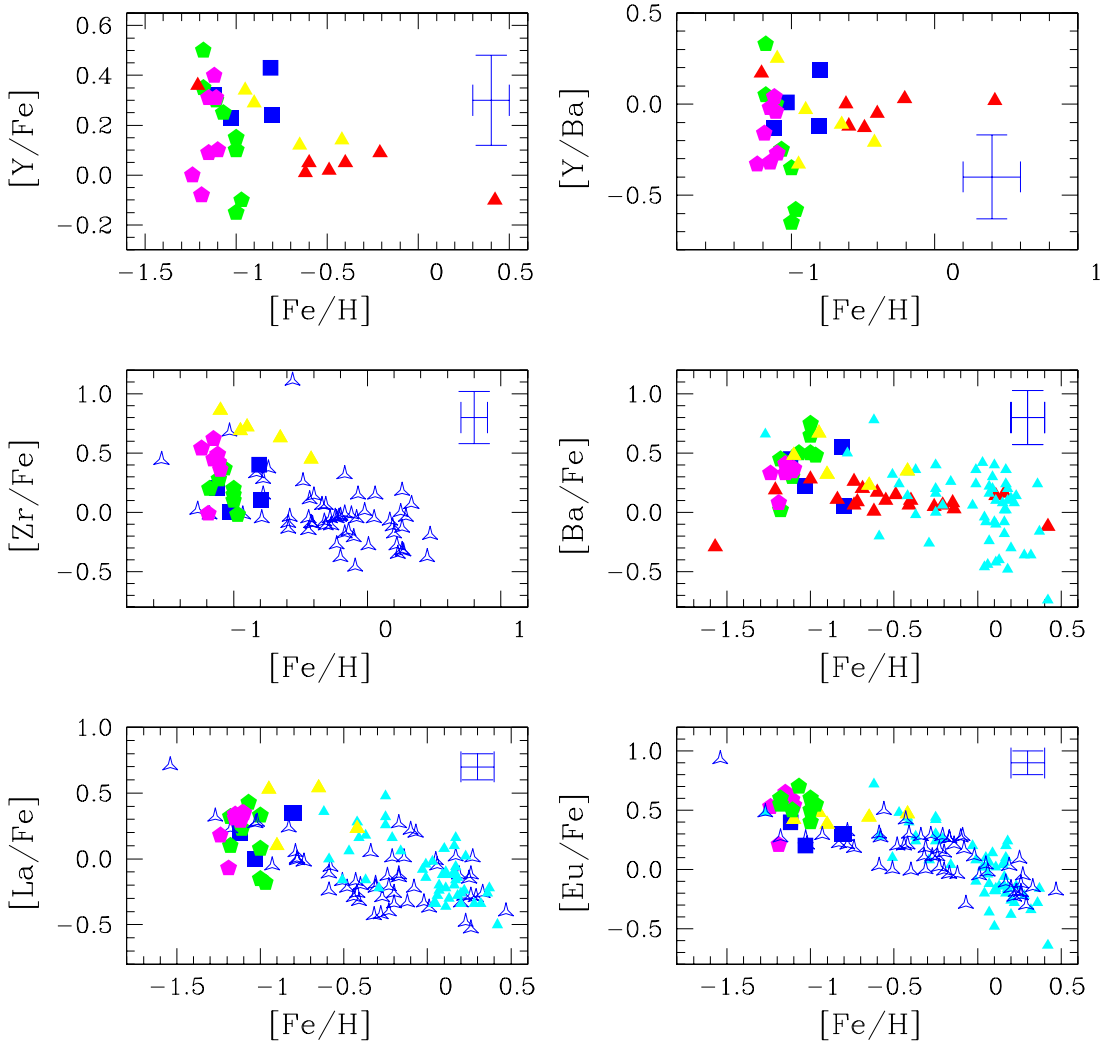

2014), indicating that these two clusters that are located in the central parts of the Galactic bulge may be of similar origin.

The abundances in the earliest globular clusters can reveal the nature of the first stars and also the location at which they formed in the Galaxy. It appears to be of great importance to further investigate this and other such clusters in terms of metallicity, abundances, kinematics, orbits, and ages.

Acknowledgements. BB, EC, AV, CSM, HE, and EB acknowledge grants and fellowships from CNPq, Capes and Fapesp. SO acknowledges the financial support from the Università di Padova and from the Italian Ministero dell'Università e della Ricerca Scientifica e Tecnologica (MURST), Italy. DM acknowledges support from the BASAL Center for Astrophysics and Associated Technologies PFB-06 and FONDECYT Project 1130196. MZ acknowledges FONDECYT Project 1150345. DM and MZ also acknowledge support from the Millennium Institute of Astrophysics MAS IC-12009.

References

Allende Prieto, C., Lambert, D.L., Asplund, M. 2001, ApJ, 556, L63
Alonso, A., Arribas, S., Martínez-Roger, C. 1998, A&AS, 131, 209
Alonso, A., Arribas, S., Martínez-Roger, C. 1999, A&AS, 140, 261 (AAM99)
Arcones, A., Thielemann, F.-K. 2013, Journal of Phys. G: Nuclear and Particle Physics, 40, issue 1, article id. 013201
Asplund, M., Grevesse, N., Sauval, A.J., Scott, P. 2009, ARA&A, 47, 481
Ballester, P. and Modigliani, A. and Boitquin, O. et al. 2000, Msngr, 101, 31B
Barbuy, B., Bica, E., Ortolani, S. 1998, A&A, 333, 117
Barbuy, B., Zoccali, M., Ortolani, S., et al. 2006, A&A, 449, 349
Barbuy, B., Zoccali, M., Ortolani, S., et al. 2007, AJ, 134, 1613

Barbuy, B., Perrin, M.-N., Katz, D. et al. 2003, A&A, 404, 661
Barbuy, B., Zoccali, M., Ortolani, S., et al. 2009, A&A, 507, 405
Barbuy, B., Chiappini, C., Cantelli, E. et al. 2014, A&A, 570, A76
Bellini, A., Vesperini, E., Piotto, G. et al. 2015, ApJ, 810, L13
Bensby, T., Yee, J.C., Feltzing, S. et al. 2013, A&A, 549, A147
Bessell, M.S. 1979, PASP, 91, 589
Bica, E., Ortolani, S., Barbuy, B. 2016, PASA, in press, ArXiv:151007834B
Bisterzo, S., Travaglio, C., Gallino, R. et al. 2014, ApJ, 787, 10
Carpenter, J.M. 2001, AJ, 121, 2851
Carretta, E., Bragaglia, A., Gratton, R., Lucatello, S. 2009, A&A, 505, 139
Cayrel, R. 1988, in IAU Symposium, Vol. 132, The Impact of Very High S/N Spectroscopy on Stellar Physics, ed. G. Cayrel de Strobel & M. Spite, 345
Cayrel, R., Depagne, E., Spite, M. et al. 2004, A&A, 416, 1117
Cescutti, G., Matteucci, F., Lanfranchi, G.A., McWilliam, A. 2008, A&A, 491, 401
Cescutti, G., Chiappini, C., Hirschi, R., Meynet, G., Frischknecht, U. 2013, A&A, 553, A51
Cescutti, G., Chiappini, C. 2014, A&A, 565, A51
Chiappini, C. 2013, AN, 334, 595
Chiappini, C., Hirschi, R., Meynet, G. et al. 2006, A&A, 449, L27
Chiappini, C., Frischknecht, U., Meynet, G. et al. 2011, Nature, 472, 454 (C11)
Coelho, P., Barbuy, B., Meléndez, J., Schiavon, R.P., Castilho, B.V. 2005, A&A, 443, 735
Davidge, T.J. 2000, ApJS, 126, 105
Dean, J.F., Warpen, P.R., Cousins, A.J.: 1978, MNRAS, 183, 569
Dékány, I., Minniti, D., Catelan, M. et al. 2013, ApJ, 776, L19
Dekker, H. and D'Odorico, S. and Kaufer, A. and Delabre, B. and Kotzlowski, H. 2000, SPIE, 4008, 534D
Dufay, J., Berthier, P., Morignat, B. 1954, Publications of the Observatoire de Haute-Provence, 3, no. 17
Frischknecht, U., Hirschi, R., Thielemann, F.-K. 2012, A&A, 538, L2
Frischknecht, U., Hirschi, R., Pignatari, M. et al. 2016, MNRAS, 456, 1803
García-Perez, A., Cunha, K., Shetrone, M. et al. 2013, ApJ, 767, L9
Gran, F., Minniti, D., Saito, R.K. et al. 2016, A&A, submitted
Gratton, R.G., Carretta, E., Bragaglia, A. 2012, A&ARv, 20, 50
Grevesse, N. & Sauval, J.N. 1998, SSRev, 35, 161
Grevesse, N., Asplund, M., Scott, P., Sauval, A.J. 2015, A&A, 573, A27
Gonzalez, O.A., Rejkuba, M., Zoccali, M. et al. 2011, A&A, 530, A54
Gustafsson, B., Edvardsson, B., Eriksson, K. et al. 2008, A&A, 486, 951
Hekker, S., Snellen, I.A.G., Aerts, C. et al. 2008, A&A, 480, 215
Hill, V., Lecureur, A., Gómez, A. et al. 2011, A&A, 534, A80
Howes, L.M., Asplund, M., Casey, A.R. et al. 2014, MNRAS, 445, 4241
Howes, L.M., Casey, A.R., Asplund, M. et al. 2015, Nature, 527, 484
Johnson, C.I., Rich, R.M., Kobayashi, C., Fulbright, J.P. 2012, ApJ, 749, 175
Kunder, A., Koch, A., Rich, R.M. et al. 2012, AJ, 143, 57
Lee, Y.-W. 1992, AJ, 104, 1780
Lodders, K., Palme, H., Gail, H.-P. 2009, Landolt-Börnstein - Group VI Astronomy and Astrophysics Numerical Data and Functional Relationships in Science and Technology Volume 4B: Solar System. Edited by J.E. Trümper, 2009, 4.4., 44
Malavolta, L., Piotto, G., Bedin, L.R. et al. 2015, MNRAS, 454, 2621
Martin, W.C., Fuhr, J.R., Kelleher, D.E., et al. 2002, NIST Atomic Database (version 2.0), http://physics.nist.gov/asd. National Institute of Standards and Technology, Gaithersburg, MD.
Meléndez, J., Barbuy, B., 2009, A&A, 497, 611
Meynet, G., Maeder, A., Eggenberger, P. et al. 2015, ArXiv:151200767M
Minniti, D. 1995, A&A, 303, 468
Modigliani, A., Mulas, G., Porceddu, I. et al. 2004, in *The Messenger*, 118, 8.
Montes, F., Beers, T.C., Cowan, J.J. et al. 2007, ApJ, 671, 1685
Ness, M., Freeman, K., Athanassoula, E. et al. 2013a, MNRAS, 430, 836
Niu, P., Cui, W., Zhang, B. 2015, ApJ, 813, 56
Ortolani, S., Bica, E., Barbuy, B. 1997, MNRAS, 284, 692
Ortolani, S., Barbuy, B., Momany, Y. et al. 2011, ApJ, 737, 31
Phillips, J.G., Davis, S.P. 1968, The Swan system of the C_2 molecule (U. of California Press)
Pietrukowicz, P., Udalski, A., Soszuński, I. et al. 2012, ApJ, 750, 169
Pietrukowicz, P., Kozlowski, S., Skowron, J. et al. 2015, ApJ, 811, 113
Piskunov, N., Kupka, F., Ryabchikova, T. et al.
Prochaska, J. X., McWilliam, A. 2000, 537, L57
Renzini, A., D'Antona, F., Cassisi, S. et al. 2015, MNRAS, 454, 4197
Roederer, I.U., Cowan, J.J., Karakas, A.I. et al. 2010, ApJ, 724, 975
Rieke, G.H., Lebofsky, M.J., 1985, ApJ, 288, 618
Rojas-Arriagada, A., Recio-Blanco, A., Hill, V. et al. 2014, A&A, 569, A103
Rossi, L., Ortolani, S., Barbuy, B., Bica, E., Bonfanti, A. 2015, MNRAS, 450, 3270
Rossi, L., Ortolani, S., S. Casotto, Barbuy, B., Bica, E. 2016, MNRAS, submitted
Saha, K., Martinez-Valpuesta, I., Gerhard, O. 2012, MNRAS, 421, 333
Saito, R. et al. (VVV collaboration) 2012, A&A, 537, 107
Siqueira-Mello, C., Chiappini, C., Barbuy, B. et al. 2016, A&A, submitted
Skrutskie, M., Cutri, R.M., Stiening, R., et al. 2006, AJ, 131, 1163
Soto, M., Barbá, R., Gunthardt, G., Minniti, D., Lucas, P. et al. 2013, A&A, 552, A101
Steffen, M., Prakapavicius, D., Caffau, E. et al. 2015, A&A, 583, A57
Stephens, A.W., Frogel, J.A. 2004, AJ, 127, 925 bibitem[] Travaglio, C., Gallino, R., Arnone, E. et al. 2004, ApJ, 601, 864
Truran, J.W. 1981, A&A, 97, 391
van der Swaelmen, M. 2013, A&A, 560, A44
van der Swaelmen, M., Barbuy, B., Hill, V. et al. 2016, A&A, in press, ArXiv: 151103919V
Walker, A.R., Terndrup, D. 1991, ApJ, 378, 119
bibitem[] Wanajo, S., Ishimaru, Y. 2006, Nucl. Phys. A, 777, 676
Yong, D., Alves-Brito, A., Da Costa, G. et al. 2014, MNRAS, 439, 2638
Zoccali, M., Lecureur, A., Hill, V. et al. 2008, A&A, 486, 177

Appendix A: Equivalent widths and atomic data

Table 7. Abundance ratios [X/Fe] of alpha-elements O, Mg, Si, Ca, Ti, and atomic parameters.

Species	λ (Å)	χ_{ex} (eV)	log gf	2115	2461	2939	3514	5037	5485
SiI	5665.555	4.920417	−2.04	+0.1	+0.2	+0.2	+0.3	0.0	+0.2
SiI	5666.690	5.616073	−1.74	—	—	—	+0.3	+0.1	+0.2
SiI	5690.425	4.929980	−1.87	+0.3	+0.2	+0.3	+0.3	+0.2	+0.0
SiI	5948.545	5.082689	−1.30	+0.4	+0.4	+0.5	+0.2	+0.3	+0.2
SiI	6142.494	5.619572	−1.50	+0.3	+0.5	+0.25	—	+0.2	+0.1
SiI	6145.020	5.616073	−1.45	+0.3	+0.3	+0.2	—	+0.1	+0.3
SiI	6155.142	5.619572	−0.85	+0.2	+0.2	+0.4	+0.4	+0.2	—
SiI	6237.328	5.613910	−1.01	+0.2	+0.2	+0.3	+0.2	+0.2	+0.1
SiI	6243.823	5.616073	−1.30	+0.2	—	+0.3	+0.4	+0.1	—
SiI	6414.987	5.871240	−1.13	+0.3	+0.4	+0.4	+0.3	+0.4	+0.2
SiI	6721.844	5.862872	−1.17	+0.2	+0.20	+0.4	+0.4	+0.2	+0.0
CaI	5601.277	2.525852	−0.52	+0.0	+0.0	+0.0	−0.1	+0.0	−0.3
CaI	5867.562	2.932710	−1.55	+0.1	+0.1	+0.0	+0.3	+0.0	—
CaI	6102.723	1.879467	−0.79	+0.3	+0.1	+0.1	−0.2	+0.2	+0.0
CaI	6122.217	1.885935	−0.20	+0.0	+0.1	+0.0	+0.0	+0.2	+0.1
CaI	6161.295	2.523157	−1.02	+0.3	+0.1	+0.4	+0.2	+0.2	+0.0
CaI	6162.167	1.899063	−0.09	+0.3	+0.1	+0.1	+0.1	+0.2	+0.0
CaI	6166.440	2.521433	−0.90	+0.3	+0.0	+0.4	+0.1	+0.3	+0.0
CaI	6169.060	2.523157	−0.54	+0.3	+0.1	+0.1	+0.2	+0.4	+0.1
CaI	6169.564	2.525852	−0.27	+0.3	+0.1	+0.2	+0.0	+0.2	+0.0
CaI	6439.080	2.525852	+0.30	+0.3	+0.0	+0.1	+0.0	+0.4	+0.1
CaI	6455.605	2.523157	−1.35	+0.3	+0.1	+0.4	+0.2	+0.4	+0.0
CaI	6464.679	2.525852	−2.10	+0.4	+0.4	>+0.5	—	+0.2	—
CaI	6471.668	2.525852	−0.59	+0.3	+0.2	+0.3	+0.2	+0.4	+0.3
CaI	6493.788	2.521433	0.00	+0.3	−0.1	+0.1	+0.0	+0.3	+0.0
CaI	6499.654	2.523157	−0.85	+0.3	+0.0	+0.3	+0.1	+0.2	+0.0
CaI	6572.779	0.00	−4.32	+0.5	0.0	+0.3	+0.2	+0.3	+0.0
CaI	6717.687	2.709192	−0.61	+0.4	+0.2	+0.5	+0.3	+0.5	+0.1
TiI	5689.459	2.296971	−0.47	+0.2	—	—	+0.1	—	—
TiI	5866.449	1.066626	−0.84	+0.1	+0.0	+0.2	+0.0	+0.3	—
TiI	5922.108	1.046078	−1.46	+0.3	+0.2	+0.4	+0.1	+0.0	—-
TiI	5941.750	1.052997	−1.53	+0.2	+0.2	+0.3	+0.2	+0.2	+0.2
TiI	5965.825	1.879329	−0.42	+0.3	+0.2	+0.3	+0.1	+0.1	+0.0
TiI	5978.539	1.873295	−0.53	+0.3	+0.1	+0.2	+0.2	+0.2	+0.0
TiI	6064.623	1.046078	−1.94	+0.3	+0.2	+0.4	+0.2	+0.3	—
TiI	6091.169	2.267521	−0.42	+0.3	+0.2	+0.3	+0.3	+0.0	+0.3
TiI	6126.214	1.066626	−1.43	+0.3	+0.2	+0.3	+0.2	+0.2	+0.0
TiI	6258.110	1.443249	−0.36	+0.1	+0.0	+0.3	+0.0	+0.1	−0.1
TiI	6261.106	1.429852	−0.48	+0.3	+0.1	+0.2	+0.0	+0.0	−0.1
TiI	6303.767	1.443249	−1.57	+0.3	+0.15	+0.35	+0.3	+0.2	+0.2
TiI	6312.240	1.460236	−1.60	+0.3	+0.3	+0.4	+0.2	+0.1	—
TiI	6336.113	1.443249	−1.74	+0.1	—	+0.2	+0.2	+0.0	—
TiI	6508.150	1.429852	−2.05	+0.2	+0.20	+0.2	+0.3	+0.2	—
TiI	6554.238	1.443249	−1.22	+0.1	+0.0	+0.2	+0.2	+0.1	−0.15
TiI	6556.077	1.460236	−1.07	+0.2	+0.2	+0.3	+0.1	+0.1	+0.0
TiI	6599.113	0.899612	−2.09	+0.3	+0.2	+0.4	+0.2	+0.5	+0.3
TiI	6743.127	0.899612	−1.73	+0.3	+0.1	+0.3	+0.3	+0.1	+0.2
TiII	5418.751	1.581911	−2.13	+0.4	+0.0	+0.1	+0.0	+0.1	+0.0
TiII	6491.580	2.061390	−2.10	+0.4	+0.2	+0.3	+0.3	+0.5	+0.1
TiII	6559.576	2.047844	−2.35	+0.4	+0.3	+0.3	+0.2	+0.5	+0.3
TiII	6606.970	2.061390	−2.85	+0.4	+0.2	+0.2	+0.25	+0.1	+0.1

Table 8. Central wavelengths, log gf and abundances of heavy elements.

species	λ (Å)	χ_{ex} (eV)	$gf_{adopted}$	2115	2461	2939	3514	5037	5485	HP1-2	HP1-3
EuII	6645.064	1.379816	+0.12	+0.50	+0.50	+0.70	+0.60	+0.60	+0.55	+0.40	+0.55
BaII	6141.713	0.703636	−0.076	+0.50	+0.30	+0.50	−0.10	+0.70	+0.50	+0.50	+0.50
BaII	6496.897	0.604321	−0.32	+0.50	+0.30	+0.50	+0.10	+0.80	+0.40	+0.80	+0.45
LaII	6262.287	0.403019	−1.60	+0.40	+0.30	+0.50	+0.30	+0.10	—	—	—
LaII	6320.376	0.172903	−1.56	+0.30	+0.00	+0.30	+0.25	+0.00	—	−0.30	−0.15
LaII	6390.477	0.321339	−1.41	+0.30	+0.40	+0.50	+0.40	+0.10	+0.10	0.00	−0.20
YI	6435.004	0.065760	−0.82	+0.20	+0.30	+0.20	+0.50	+0.20:	+0.50	−0.15	—
YII	6795.414	1.738160	−1.19	+0.1	+0.30	+0.30	+0.20	+0.00	—	−0.15	−0.10
ZrI	6127.475	0.153855	−1.18	+0.10	+0.00	+0.40	+0.40	+0.20	—	—	+0.10
ZrI	6134.585	0.00	−1.43	+0.10	+0.50	+0.30	—	+0.20	—	+0.20:	0.00
ZrI	6140.535	0.00	+0.10	—	+0.50	—	—	—	(+0.70)	—	
ZrI	6143.252	0.070727	−1.50	+0.10	+0.10	+0.40	+0.00	+0.00	+0.30:	—	−0.15
SrI	6503.989	2.258995	+0.26	+0.30	—	+0.30:	—	+0.30::	—	+0.50	+0.30:
SrI	6791.016	1.775266	−0.73	+0.80:	—	—	—	+0.50::	—	—	—

Table 10. Mean abundances of C, N, odd-Z elements Na, Al, and α-elements O, Mg, Si, Ca, Ti, and heavy elements Y, Sr, Zr, Ba, La, and Eu. Mean values for NGC 6522 are given in the last column.

[X/Fe]	2115	2461	2939	3514	5037	5485	HP1-2	HP1-3	Mean	NGC 6522
C	≤+0.00	≤+0.00	≤+0.00	≤+0.00	≤+0.00	≤+0.00	+0.00	+0.00	+0.00	−0.03
N	≤+0.70	+≤0.50	≤+0.50	≤+0.80	≤+0.50	≤+0.50	+0.50	+0.20	+0.53	+0.67
O	+0.40	+0.50	+0.50	+0.40	+0.35	+0.40	+0.30	+0.30	+0.40	+0.36
Na	+0.03	−0.30	−0.23	−0.10	−0.10	−0.30	−0.05	−0.20	−0.16	+0.05
Al	−0.15	+0.05	+0.05	+0.08	+0.20	+0.20	−0.28	+0.18	+0.04	+0.20
Mg	+0.30	+0.35	+0.65	+0.35	+0.33	+0.40	+0.15	+0.33	+0.36	+0.23
Si	+0.25	+0.31	+0.33	+0.31	+0.20	+0.15	+0.30	+0.30	+0.27	+0.13
Ca	+0.28	+0.11	+0.21	+0.11	+0.26	+0.04	−0.04	+0.10	+013	+0.13
TiI	+0.26	+0.16	+0.28	+0.17	+0.16	+0.06	+0.07	+0.08	+0.16	+0.04
TiII	+0.40	+0.18	+0.23	+0.19	+0.31	+0.13	+0.10	+0.15	+0.21	+0.17
Y	+0.15	+0.30	+0.25	+0.35	+0.10	+0.50	-0.15	−0.1	+0.18	+0.31
Zr	+0.15	−0.10	+0.28	+0.37	+0.20	+0.15	—	−0.02	+0.15	+0.18
Sr	+0.55:	—	+0.30	—	+0.40	—	+0.50:	+0.30:	+0.41:	+0.23
Ba	+0.50	+0.30	+0.50	+0.00	+0.75	+0.45	+0.65	+0.47	+0.46	+0.32
La	+0.33	+0.23	+0.43	+0.32	+0.08	+0.10	−0.15	−0.18	+0.23	—
Eu	+0.50	+0.50	+0.70	+0.60	+0.60	+0.55	+0.40	+0.55	+0.15	+0.30
Ba/Eu	0.0	−0.20	−0.20	−0.60	+0.15	−0.10	+0.25	−0.08	+0.31	–
v_r (km s^{-1})	+41.0	+41.0	+46.0	+35.0	+41.0	+34.0	+44.6	+44.0		

Table A.1. Fe I and Fe II lines, their wavelengths, excitation potential (eV), oscillator strengths from NIST and VALD3 for Fe I and Fuhr & Wiese (2006) and Meléndez & Barbuy (2009) for Fe II, and equivalent widths (mÅ).

species	λ(Å)	χ_{ex}(eV)	log gf$_{NIST}$	log gf$_{VALD}$	log gf$_{adopted}$	2115	2461	2939	3514	5037	5485
			FW06	MB09							
FeII	5991.38	3.15	−3.65	−3.54	−3.54	—-	33.8	—-	24.6	27.5	26.2
FeII	6149.25	3.89	−2.84	−2.69	−2.69	26.3	32.9	23.5	31.4	22.3	33.0
FeII	6247.56	3.89	−2.43	−2.30	−2.30	24.1	38.9	27.8	—-	28.0	46.1
FeII	6416.93	3.89	−2.88	−2.64	−2.64	24.9	26.0	23.1	20.6	—-	33.5
FeII	6432.68	2.89	−3.50	−3.57	−3.57	33.6	41.7	32.4	34.1	29.2	45.5
FeII	6516.08	2.89	−3.372	−3.31	−3.31	45.7	59.9	47.9	51.7	44.0	64.0
FeI	5525.544	4.231	—	−1.084	−1.084	—-	37.7	—-	—	—-	40.5
FeI	5543.360	4.218	—	−1.140	−1.11	—-	45.5	—-	—	62.1	35.2
FeI	5554.894	4.549	—	−0.440	−0.440	—-	67.9	67.8	—	74.4	48.6
FeI	5560.211	4.435	—	−1.190	−1.16	39.4	29.5	41.3	—	34.0	22.5
FeI	5567.391	2.609	—	−2.564	−2.67	75.8	58.1	77.6	—	68.0	51.2
FeI	5618.632	4.209	—	−1.276	−1.276	38.3	30.5	49.5	—	34.1	34.6
FeI	5619.595	4.387	—	−1.700	−1.67	31.1	—-	27.5	—	23.6	—-
FeI	5633.946	4.991	—	−0.270	−0.32	44.7	44.7	56.6	—	38.4	33.6
FeI	5638.262	4.220	—	−0.870	−0.84	63.4	62.2	76.1	—	60.6	34.9
FeI	5641.434	4.256	—	−1.180	−1.15	58.8	48.3	59.5	—	60.1	39.2
FeI	5653.865	4.387	—	−1.640	−1.61	26.2	—-	—-	—	20.9	—-
FeI	5679.023	4.652	—	−0.920	−0.90	—-	31.8	34.5	—-	42.5	36.4
FeI	5701.544	2.559	—	−2.216	−2.216	—-	—-	—-	—-	94.0	70.7
FeI	5706.096	4.283	—	−3.012	−3.012	—-	58.3	—-	—-	—-	—-
FeI	5717.833	4.284	—	−1.130	−1.10	28.8	28.7	36.2	46.4	42.9	37.0
FeI	6056.005	4.733	—	−0.460	−0.460	48.8	42.8	54.7	—	50.8	34.6
FeI	6078.491	4.796	—	−0.321	−0.321	59.3	49.5	52.0	55.9	56.5	44.3
FeI	6079.008	4.652	−1.100	−1.120	−1.100	30.8	31.8	26.5	24.2	31.4	—-
FeI	6082.710	2.223	−3.573	−3.573	−3.573	67.6	48.2	61.2	50.9	53.8	24.5
FeI	6093.643	4.608	−1.470	−1.599	−1.470	20.8	—-	—-	—-	24.2	—-
FeI	6096.664	3.984	−1.880	−1.930	−1.88	34.4	23.8	28.9	23.1	30.5	—-
FeI	6151.617	2.176	−3.299	−3.299	−3.299	80.9	76.2	81.1	78.2	76.2	47.5
FeI	6157.728	4.076	−1.22	−1.260	−1.22	69.6	60.8	72.4	40.0	64.0	41.8
FeI	6165.360	4.143	−1.474	−1.474	−1.474	53.1	44.2	47.3	49.0	49.7	42.2
FeI	6180.203	2.728	−2.649	−2.586	−2.649	84.4	74.9	87.3	79.7	79.0	61.7
FeI	6187.989	3.943	−1.67	−1.720	−1.67	51.7	39.9	56.7	46.5	43.2	23.3
FeI	6200.313	2.609	−2.437	−2.437	−2.437	—-	—-	—-	97.7	—-	—-
FeI	6219.281	2.198	−2.433	−2.433	−2.43	—-	—-	—-	—-	—-	97.9
FeI	6226.734	3.884	—	−2.220	−2.220	—-	—-	21.6	—-	—-	—-
FeI	6229.226	2.845	−2.805	−2.805	−2.805	26.8	36.9	51.7	45.6	41.5	22.8
FeI	6240.646	2.223	−3.173	−3.233	−3.173	75.7	54.9	74.6	—	70.0	37.3
FeI	6246.318	3.603	−0.877	−0.733	−0.877	—-	68.6	—-	—	90.8	80.9
FeI	6265.132	2.176	−2.550	−2.550	−2.550	—-	—-	—-	—-	—-	95.5
FeI	6270.223	2.858	−2.609	−2.464	−2.609	76.8	64.5	68.7	60.7	66.5	44.1
FeI	6271.278	3.332	−2.703	−2.703	−2.703	24.8	20.8	24.9	—-	—-	—-
FeI	6302.494	3.686	—	−0.973	−0.973	84.7	77.9	83.7	—	85.0	62.2
FeI	6311.500	2.832	−3.141	−3.141	−3.141	48.8	25.9	42.8	30.4	39.0	—-
FeI	6315.306	4.143	−1.232	−1.232	−1.232	62.8	53.5	61.0	57.3	56.0	38.9
FeI	6315.811	4.076	−1.66	−1.710	−1.66	40.0	—-	40.0	33.0	36.8	24.4
FeI	6322.685	2.588	−2.426	−2.426	−2.426	—-	95.1	—-	95.8	—-	82.9
FeI	6336.823	3.686	−0.856	−0.856	−0.856	—-	98.3	—-	—	—-	88.8
FeI	6344.148	2.433	−2.923	−2.923	−2.92	—-	87.8	—-	88.8	91.0	62.1
FeI	6355.028	2.845	−2.291	−2.350	−2.291	88.6	71.3	79.8	—	78.3	51.7
FeI	6380.743	4.186	−1.376	−1.376	−1.376	50.0	45.3	47.4	33.7	51.1	31.3
FeI	6392.538	2.279	—	−4.030	−4.030	42.5	21.6	38.0	24.3	32.6	—-
FeI	6408.017	3.686	−1.018	−1.018	−1.018	96.7	86.0	87.8	84.4	85.4	77.1

FeI	6411.648	3.654	−0.718	−0.595	−0.718	—-	—-	—-	—-	—-	98.9
FeI	6419.949	4.733	−0.27	−0.240	−0.27	66.7	58.8	65.4	63.8	66.4	47.0
FeI	6469.192	4.835	−0.81	−0.770	−0.81	—-	26.9	—-	—-	38.5	—-
FeI	6475.624	2.559	−2.942	−2.942	−2.942	76.4	64.5	81.4	68.6	83.4	50.4
FeI	6481.870	2.279	−2.984	−2.984	−2.984	96.4	79.4	98.3	89.2	—-	69.9
FeI	6498.938	0.958	−4.687	−4.699	−4.687	—-	80.0	—-	94.8	—-	58.9
FeI	6518.366	2.832	−2.298	−2.460	−2.298	82.0	68.5	86.8	—	76.6	53.1
FeI	6569.214	4.733	−0.450	−0.420	−0.450	63.4	60.5	65.2	67.2	63.1	46.2
FeI	6574.226	0.990	−5.004	−5.023	−5.004	93.5	62.3	89.5	78.8	80.8	44.5
FeI	6575.016	2.588	−2.710	−2.710	−2.710	95.2	79.8	93.2	85.7	83.3	65.3
FeI	6581.209	1.485	−4.679	−4.679	−4.679	56.8	28.3	58.4	39.7	42.2	21.7
FeI	6593.870	2.433	−2.422	−2.422	−2.422	—-	—-	—-	—-	—-	92.8
FeI	6597.559	4.796	−1.050	−1.070	−1.05	29.5	20.6	26.4	31.7	26.3	—-
FeI	6608.025	2.279	—	−4.030	−4.030	39.3	—-	38.0	27.9	35.9	—-
FeI	6609.110	2.559	−2.692	−2.692	−2.692	95.4	77.9	93.0	87.7	82.7	61.8
FeI	6627.544	4.549	—	−1.680	−1.680	20.5	—-	—-	—-	—-	—-